

Effect of local geometry on magnetic property of nitric oxide on Au(110)-(1×2)H. Koshida , H. Okuyama *, S. Hatta, and T. Aruga*Department of Chemistry, Graduate School of Science, Kyoto University, Kyoto 606-8502, Japan*E. Minamitani *Institute for Molecular Science, Okazaki 444-8585, Japan* (Received 24 November 2020; revised 2 February 2021; accepted 23 March 2021; published 12 April 2021)

We investigate the effect of local geometry and environment on the electronic spin of nitric oxide (NO) on Au(110)-(1×2) using scanning tunneling microscopy/spectroscopy, density functional theory, and numerical renormalization group calculations. The molecules adsorb on the bridge or on-top sites, and the Kondo resonance is observed only for the latter. This indicates that the local geometry influences the spin state of NO on the surface. The Kondo resonance is accompanied by enhanced satellite peaks due to the interplay with vibrational excitation. In addition, we find that the Kondo resonance appears as a peak or a dip, depending on the local environment of the molecule. The calculations reveal that the NO/Au(110) system is represented by a two-orbital Anderson model, where the $2\pi^*$ orbitals compete for the unpaired electron to host the Kondo resonance. We propose that a subtle interaction between the NO molecules may play a critical role in determining the host of Kondo resonance and, consequently, the spectral shape.

DOI: [10.1103/PhysRevB.103.155412](https://doi.org/10.1103/PhysRevB.103.155412)**I. INTRODUCTION**

The spin polarization of a free nitric oxide (NO) molecule arises from the unpaired electron in the $2\pi^*$ orbital. Whether the spin survives or not on metal surfaces is a fundamental issue for understanding the coupling of spin degrees of freedom with condensed matter. Yoshimori [1] examined the two-photon photoemission data of NO on Cu(111) [2] by using a many-body-model Hamiltonian and proposed that the magnetic moment exists on the surface. In addition, density functional theory (DFT) has been employed to address this issue, and the results indicate that NO retains its magnetic moment on Ag(111) [3], whereas the magnetic moment is lost on Pt(111) [4] and other transition metal surfaces [5]. The hybridization between the $2\pi^*$ orbital and metal d states is significant on transition metal surfaces, resulting in the loss of the magnetic moment.

It is well known that itinerant metal electrons may screen a localized spin of magnetic atom on low-temperature surfaces. This many-body correlation effect gives rise to a zero-bias resonance (Kondo resonance) peak or dip in scanning tunneling spectroscopy (STS) measurements [6–8]. Therefore, Kondo resonance observation suggests the presence of a localized spin on adatoms, forming a singlet state with electrons in the metal. Kondo resonance has also been observed for a variety of molecules, ranging from metal-cyanide complexes [9–16] and magnetic molecules [17–20] to pure organic materials [21–25]. Requist *et al.* [19] observed Kondo resonance for NO on Au(111) and proposed that the radical character of NO is retained on the surface, with its spin moment screened by

the conduction electron in the metal. However, the correlation of the spin state of adsorbed NO with the local geometry on metal surfaces has not been investigated thoroughly. The interaction of NO with metal surfaces is complex, giving rise to a variety of adsorbed states. The adsorption results in, e.g., upright or flat-lying configurations, depending on the temperature and coverage, even for one and the same surface [26,27]. Thus, it is essential to probe the spin at the level of individual molecules. In this context, the scanning tunneling microscope (STM) is an ideal tool, enabling the observation and characterization of adsorbed NO molecules in a single-molecule limit [28]. Therefore, NO/metal systems may serve as a useful testbed for studying the interplay between spin states and the local environment on surfaces.

In this study we investigated the local geometry of NO on Au(110)-(1×2), and its influences on the inherent magnetic property of NO, using STM in conjunction with DFT and numerical renormalization group (NRG) calculations. The reconstructed Au(110) surface allows for various adsorption states of NO, and their relatively weak interaction is ideal for studying the magnetic property of NO. We found that NO molecules adsorb on the bridge and on-top sites. The on-top species exhibited Kondo resonance, while the bridge species did not, suggesting the existence of the spin for the former. Because the molecular axis is tilted from the surface normal, the degeneracy of the $2\pi^*$ orbitals is lifted. Therefore, the two orbitals compete for an unpaired electron that causes Kondo resonance. The NRG and DFT calculations suggested that the environment of NO molecules plays a critical role in determining the Kondo channel. In addition, we observed satellite peaks beside the Kondo resonance, which can be attributed to the vibration-assisted Kondo resonance. The satellite peaks were assigned based on the symmetry consideration, spatial

*hokuyama@kuchem.kyoto-u.ac.jp

distribution of the peak intensity, and DFT calculations of the normal modes.

II. EXPERIMENTS

The STM experiment was conducted at 4.5 K in an ultrahigh-vacuum chamber, using an electrochemically etched tungsten tip as the STM probe. The single crystalline Au(110) surface was cleaned by repeated cycles of argon ion sputtering and annealing. The clean Au(110) surface exhibited (1×2) missing-row reconstruction [29], which was routinely observed in the STM image as straight lines running along the $[1\bar{1}0]$ direction. NO gas (^{14}NO and ^{15}NO) was introduced into the chamber via a tube doser to the surface maintained at 78 K. STM images were acquired in the constant current mode at a sample bias $V_s = 50$ mV and tunneling current $I = 0.1$ nA. STS (dI/dV and d^2I/dV^2) was obtained with a lock-in technique, with a modulation voltage of 4 mV_{rms} at 560 Hz.

III. THEORY

Density functional calculations were performed by using the Vienna *ab initio* Simulation Package [30,31] with the projected augmented wave [32] method. The optB86b-vdW exchange-correlation functional [33] was used to account for the van der Waals interaction. The cutoff energy of the plane-wave basis was set to 400 eV. The first Brillouin zone was sampled by uniform $4 \times 6 \times 1$ mesh centered at the Γ point. The surface of Au(110)- (1×2) was modeled using a slab with 11 atomic layers. The supercell size in the in-plane direction was taken to 4×3 . The atomic positions except for the Au atoms in the bottom three layers were relaxed until the forces on each atom became smaller than 0.02 eV/Å. All the calculated structures were rendered by VESTA 3 [34].

We performed NRG calculations using our own developed code [35,36]. We used the logarithmic discretization parameter $\Lambda = 2.0$, and ~ 2000 low-lying eigenstates were kept in respective iterations. In the calculation of the single-particle excitation spectrum, we implemented the method proposed by Anders *et al.* [37,38], in which the NRG data from all iterations were combined to construct a complete Fock space. All NRG calculations were performed at 0 K in the present work.

IV. RESULTS

A. STM observation

Figure 1(a) shows a typical STM image of Au(110)- (1×2) exposed to NO. Individual molecules are imaged as protrusions that preferentially form chain clusters along the $[1\bar{1}0]$ direction. Isolated molecules are also observed, which are shown in Figs. 1(b) and 1(c) with the Au(110)- (1×2) lattice superimposed. The lattice is drawn using residual carbon monoxide (CO) molecules that adsorb at the on-top site [39]. The lattice indicates that the isolated molecules are located at the short-bridge site (hereafter denoted by *b*-NO). The spot is off-centered in the $[001]$ or $[00\bar{1}]$ directions, suggesting that *b*-NO adsorbs in a tilted manner.

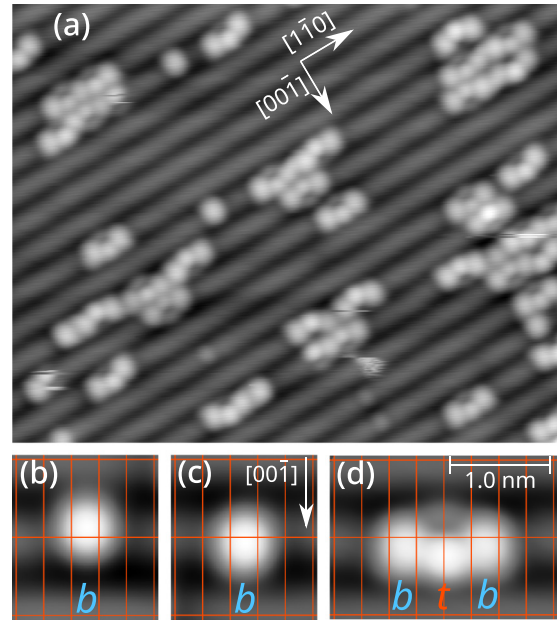


FIG. 1. (a) Typical STM image of the Au(110)- (1×2) surface exposed to NO. The molecules prefer chain formation along the $[1\bar{1}0]$ direction. Isolated molecules are also observed, as shown in (b) and (c), with the lattice superimposed. The molecules are bonded to the short-bridge site (*b*-NO). (d) Magnified image of a chain comprising three molecules. The edge molecules are identical with *b*-NO, while the center molecule is bonded to the on-top site (*t*-NO). The image size is 13.7×14.8 nm for (a).

Figure 1(d) shows a magnified image of a chain cluster comprising three molecules. The two edge molecules located at the short bridge site are identical to the *b*-NO described above. On the other hand, the center molecule is located at the on-top site (hereafter denoted by *t*-NO). The molecule appears as a pair of a large and a small protrusion, suggesting that it is also tilted along $[001]$. The two-spot image is similar to that of NO/Cu(110), which originates in the $2\pi^*$ orbital of NO [40]. A *t*-NO is never observed as a monomer and is always attached to *b*-NO, often sandwiched between two *b*-NO, as shown in Fig. 1(d). Nevertheless, the molecular interaction between *b*-NO and *t*-NO is weaker than the covalent bonding [40], which is supported by the same STM images of the *b*-NO in the isolated form and chain [Figs. 1(b)–1(d)]. This implies that molecules in the chain interact with each other via the weak interaction (e.g., van der Waals interaction).

B. STS measurement

To verify whether the localized spin remains in the NO on Au(110)- (1×2) , we conducted STS measurements. Figure 2 shows the STS measured on the three protrusions of the chain (*b*-NO and *t*-NO) and the clean surface. The tip position is shown in the image. The dI/dV for *t*-NO (purple) shows a distinct peak centered at the Fermi level, while those for *b*-NO are featureless (orange and blue curves). It is noted that the STS for isolated *b*-NO displays no feature as well. The peak half-width-half-maximum (HWHM) for *t*-NO is 14.6 ± 1.9 meV, and such a sharp peak implies that it is attributed to the Kondo resonance. This was supported by the

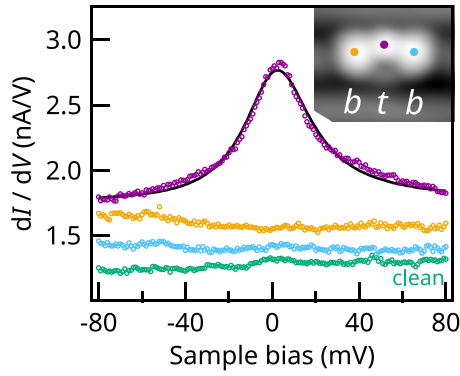


FIG. 2. dI/dV spectra recorded over b -NO (orange and blue), t -NO (purple) in the chain, and over the clean surface (green). The dI/dV for t -NO exhibits a distinct peak centered at 0 mV, while those for b -NO and the clean surface are featureless. The spectrum for t -NO was fitted to the Fano function [Eq. (1), black curve]. A linear slope was allowed for the fit. The tip height was fixed at $V_s = 100$ mV and $I = 0.1$ nA during each measurement. The spectra were vertically offset for clarity.

temperature dependence of the spectra (Fig. S1), where the Kondo temperature was determined to be 114 ± 18 K [41]. These results suggest that the molecular spin is maintained for t -NO, but quenched for b -NO. The spectra of the Kondo resonance are represented by the following Fano function:

$$dI/dV = \frac{(\epsilon + q)^2}{1 + \epsilon^2}, \quad \epsilon = \frac{V - V_0}{\Gamma}, \quad (1)$$

where V_0 and Γ are the position and HWHM of the resonance, respectively. The spectral shape is determined by the interference between the tunneling electrons from the tip to the molecular states and to the substrate, where q denotes the ratio of the two paths [8]. The solid curve in Fig. 2 shows the fit to Eq. (1). The value of q was determined to be 17 (almost the same as a Lorentz peak), which indicates that the former path is dominant. The q value also reflects the nature of the molecular orbital responsible for the Kondo resonance, as described in Sec. V A.

C. DFT calculation

We studied the structure and electronic states of NO on Au(110)-(1 \times 2) by DFT calculations. We found that the adsorption energy of the isolated bridge and on-top NO were 0.80 and 0.77 eV, respectively. For both species, the N–O axis was tilted from the surface normal along the [001] direction (Fig. S2) [41]. These results are in agreement with previous calculation [42] and consistent with the STM observation [Figs. 1(b) and 1(c)]. Next, we calculated the infinite chain structure comprised of alternating bridge and on-top NO on Au(110)-(1 \times 2), as the structure in Figs. 1(d) and 2. As well as for the isolated NO, the bridge and on-top NO are tilted along the [001] direction in the optimized structure of the chain [Figs. 3(a) and 3(b)]. The adsorption energies of the molecules are almost the same as those for the isolated NO, indicating that the interaction between the molecules in the chain is quite weak. This may contradict the preferential chain

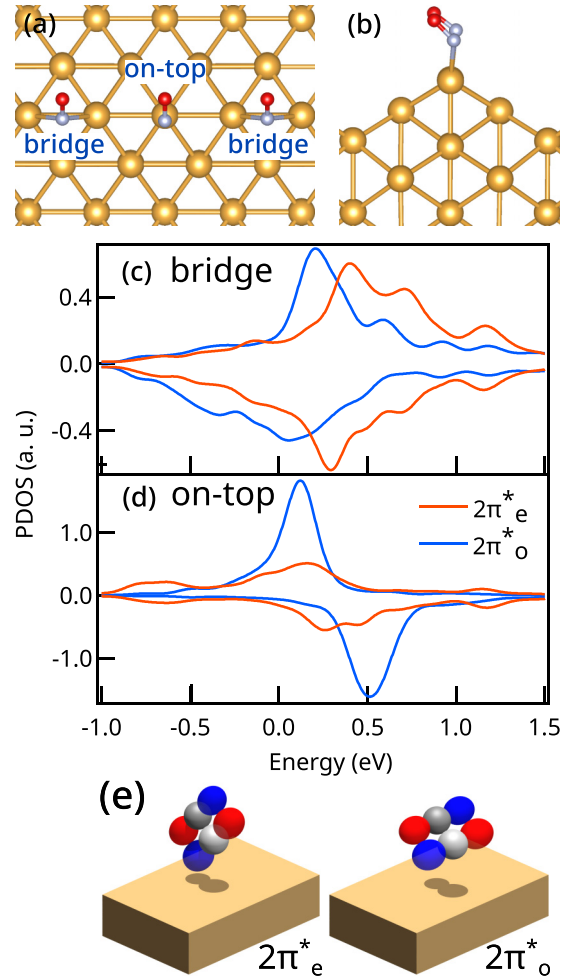


FIG. 3. (a) Top view and (b) side view of the calculated structure of the NO chain, where the bridge and on-top NO are arranged alternately. The distance between adjacent bridge and on-top NO molecules is 0.43 nm. (c, d) Spin-resolved density of states projected onto the two orbitals for (c) bridge and (d) on-top NO in the chain structure. The on-top NO maintains spin polarization, whereas the bridge NO almost does not. The sign of PDOS indicates the spin direction. (e) Schematics of the molecular orbitals of NO, $2\pi_e^*$, and $2\pi_o^*$.

formation, but may be dominated by the kinetics of the adsorption process, the details of which remain to be clarified.

Figures 3(c) and 3(d) show the spin-resolved projected density of states (PDOS) to the $2\pi^*$ orbitals of the bridge and on-top NO in the chain, respectively. Because the molecules are bonded in a tilted geometry, the degeneracy of the $2\pi^*$ orbital is lifted, giving rise to the two orbitals labeled as $2\pi_e^*$ and $2\pi_o^*$ [Fig. 3(e)]. The subscript represents the orbital symmetry (even/odd) with respect to the reflection against the plane along [001] and the surface normal. The hybridization of the orbitals with the metal state leads to a broadening of the levels and decreases in the Coulomb interactions. Figures 3(c) and 3(d) indicate that the bridge NO hybridized with substrate stronger than the on-top NO. As a result, the spin polarization of the bridge NO ($0.22 \mu_B$) becomes smaller than the on-top NO ($0.31 \mu_B$). These results indicate that the magnetic

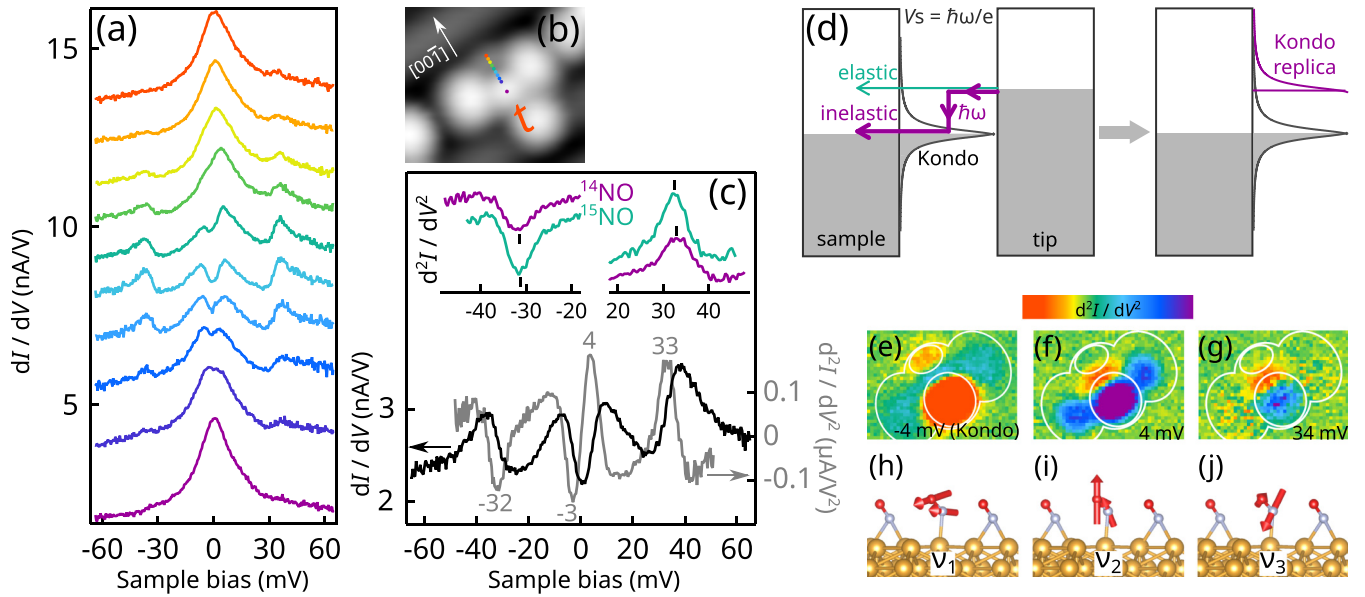


FIG. 4. (a) Series of dI/dV spectra recorded at each position over t -NO shown in (b). The Kondo peak at 0 mV is replaced by two sets of side features at ± 35 mV and ± 5 mV in the middle. (c) Bottom shows the dI/dV (black) and d^2I/dV^2 (gray) curves for the side features. The latter shows peaks (dips) at 4 mV and 33 mV (-3 mV and -32 mV). Isotope shift (^{14}NO and ^{15}NO) for the 33 (-32) mV peak (dip) is shown in the top, suggesting that the peak and dip are associated with vibrational excitation. (d) Schematic illustration of inelastic vibrational tunneling enhanced by Kondo resonance (left), and the resulting “Kondo replica” in dI/dV (right). A positive bias is assumed (the same diagram can be drawn for a negative bias). (e–g) Constant-height d^2I/dV^2 maps of (e) -4 mV (corresponding to Kondo peak), (f) 4 mV, and (g) 34 mV. The superimposed white curves indicate the contour of the molecules (b -NO, t -NO, and b -NO). The tip height was fixed at $V_s = 100$ mV and $I = 0.5$ nA over the main protrusion of t -NO. (h–j) Calculated vibrational modes of t -NO, which are totally symmetric under the C_s symmetry. (h) Hindered translation (5 meV, ν_1), (i) NO–Au stretch (25 meV, ν_2), and (j) hindered rotation (45 meV, ν_3). The image sizes are 1.9×2.2 nm for (b) and 1.1×1.5 nm for (e–g). The tip height was fixed at $V_s = 50$ mV and $I = 0.1$ nA during each measurement in (a) and (c). The spectra in (a) and the top part of (c) are vertically offset for clarity.

moment in bridge NO is suppressed, which is consistent with the fact that the Kondo resonance was observed only for t -NO.

D. Vibration-Kondo coupling of t -NO

We observed satellite peaks for t -NO, depending on the tip position. Figure 4(a) shows the dI/dV spectra for t -NO recorded with the tip position varied, as shown in Fig. 4(b). When the tip is positioned just over the larger protrusion, the dI/dV exhibits a single symmetric Kondo peak centered at 0 mV (purple curve), as shown in Fig. 2. As the tip is moved in the $[00\bar{1}]$ direction, the Kondo peak is reduced in intensity, and asymmetric satellite peaks appear at $\sim \pm 35$ mV and $\sim \pm 5$ mV (blue to green curves). Finally, with the tip positioned over the smaller protrusion, the Kondo peak revives, and the satellite peaks disappear (red curve).

To explore the origin of the satellite peaks, we studied the isotope dependence (^{14}NO and ^{15}NO). To determine the existence of the isotopic shift, we compared the peak voltage using d^2I/dV^2 , as shown in the bottom of Fig. 4(c) (gray curve). The d^2I/dV^2 peaks (dips) at 4 mV and 33 mV (-3 mV and -32 mV) correspond to the onset of the satellite peaks at ± 5 mV and ± 35 mV in the dI/dV (black curve), respectively. The top of Fig. 4(c) shows the comparison of the d^2I/dV^2 features between ^{14}NO and ^{15}NO , exhibiting the $\sim 2\%$ isotopic shift. Thus, we attribute the origin of the satellite peaks at $\sim \pm 35$ mV in the dI/dV to the vibrational excita-

tion. We note that the energy barrier to spin flip ($^2\Pi_{\frac{1}{2}} \rightarrow ^2\Pi_{\frac{3}{2}}$) is 15 meV for free NO [43,44], which does not match the peak (dip) energy. Thus, the spin excitation [45,46] is discarded as the peak (dip) origin.

The peaks are ascribed to vibrational excitation coupled with the Kondo resonance, as observed previously in the electron transport through quantum dots [47], and in the STS measurements for large organic molecules on metal surfaces [12,14,15,18,21,24,25]. The relatively small degrees of freedom of NO allow us to investigate the vibrational modes involved and the mechanism of the vibration-Kondo coupling in a rather straightforward manner. The vibrational inelastic process in the presence of Kondo resonance is qualitatively described using a simple tunneling model shown in Fig. 4(d). If eV_s matches or exceeds the vibrational energy ($V_s \geq \hbar\omega/e$), tunneling electrons can dissipate its energy to the molecule or the substrate by emitting phonons. In Kondo systems, such an inelastic electron tunneling (IET) can be coupled with Kondo resonance, which produces a “Kondo replica” in the differential conductance (vibration-assisted Kondo effect), as depicted in Fig. 4(d) [12,21,24,47]. As evident from this model, the Kondo replica has an asymmetric shape with a steep onset at the vibrational excitation, which is consistent with the satellite peaks observed in Figs. 4(a) and 4(c). This indicates that $\hbar\omega/e$ corresponds to the peak (dip) position in d^2I/dV^2 . It is also notable that the conductance increase at the onset is $\sim 50\%$, which is considerably large in comparison with that

for normal IET (a few % [48]), suggesting that the tunneling via vibrational excitation is significantly enhanced due to the large final-state density, i.e., the Kondo resonance.

A series of dI/dV spectra in Fig. 4(a) indicates that the intensities of the Kondo resonance and the vibrational satellite peaks depend critically on the tip position above the molecule. Figures 4(e)–4(g) show the d^2I/dV^2 spatial maps obtained for the chain cluster with V_s fixed at -4 mV (corresponding to the Kondo resonance), 4 mV, and 34 mV (satellite peaks in the dI/dV), respectively. The red areas correspond to the distribution of Kondo resonance and satellite peaks. As seen in Figs. 4(a) and 4(e), the Kondo resonance intensity is enhanced at the two protrusions of t -NO and suppressed in between. This reflects the local density of states of the orbital that hosts the Kondo resonance [$2\pi_e^*$ orbital [Fig. 3(e)], as described in Sec. V A]. In contrast, the satellite peaks are distributed between the protrusions, as shown in Figs. 4(a), 4(f), and 4(g).

We consider the spatial distribution and assignment of the satellite peaks based on the IET propensity rule [49–52]. The t -NO belongs to the C_s point group with the mirror plane (σ_v) along $[001]$ and $[110]$ (surface normal). The $2\pi_e^*$ orbital, which causes the Kondo resonance and contributes to electron tunneling at the Fermi level, is symmetric with respect to the reflection against σ_v (represented by the symmetry species of a'). The satellite signal has an intensity in the mirror plane [Figs. 4(f) and 4(g)], indicating that the tunneling matrix element is nonzero only when the vibrational mode is totally symmetric (a' mode). Therefore, the satellite peaks can be assigned to the normal modes illustrated in Figs. 4(h)–4(j). It is noted that internal stretch mode [$\nu(\text{N-O})$] is ruled out because the frequency lies outside the range (~ 200 meV). ν_1 is well described by the hindered translation motion along the $[001]$ direction, while ν_2 and ν_3 mainly include the Au-NO stretch and hindered rotation motion, respectively. The dI/dV peaks at ± 5 meV are assigned to ν_1 based on the frequency, and the dI/dV peaks at ± 35 meV are assigned to ν_2 and/or ν_3 . It is notable that the intensities of the vibration modes are distributed between the lobes, i.e., at the node of the $2\pi_e^*$ orbital [Figs. 4(a), 4(f), and 4(g)]. This can be rationalized by the inelastic process in which the initial state is 5σ or $6\sigma^*$, and the final state is $2\pi_e^*$ [50,52], which supports that the ν_3 (hindered rotation) is more plausible as the origin of the dI/dV peaks at ± 35 meV.

E. Metastable species produced by STM

When Au(110)-(1 \times 2) is exposed to NO at 78 K, NO is observed to exist as b -NO or t -NO, as described above. By applying a voltage pulse (~ 300 mV, 1 s) to b -NO, we observed a new species, as shown in Figs. 5(a) and 5(b). The product does not exist naturally and exhibits a characteristic combination of pear-shaped and crescent-shaped protrusions, suggesting that the $2\pi^*$ orbital contributes to the electron tunneling. This low-symmetry species (hereafter denoted as l -NO) flips between two equivalent orientations [Figs. 5(c) and 5(d)] and occasionally returns to b -NO via voltage pulses of ~ 300 mV. The STS for this species exhibits a dip structure, as shown in Fig. 5(e). We could reasonably fit the spectrum to the Fano function [Eq. (1)] and determined the q value as 0.02 (almost the same as a Lorentz dip). This result suggests

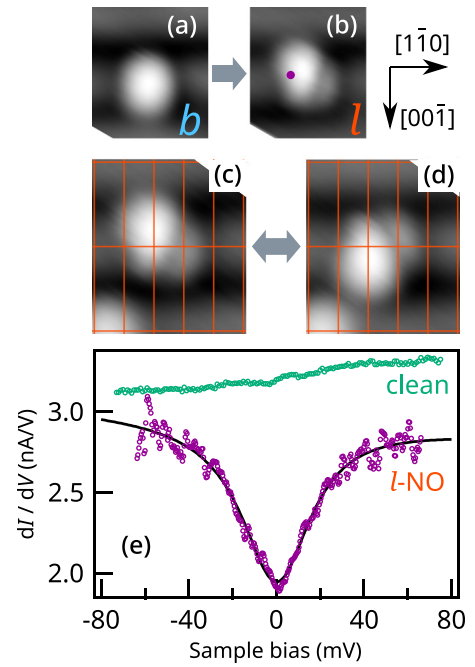


FIG. 5. (a, b) Manipulation of b -NO. By applying a voltage pulse (350 mV, 1 s) onto b -NO, the b -NO changes to the low-symmetry species denoted as l -NO. The l -NO flips along the $[001]$ direction on applying a ~ 300 mV voltage pulse, as shown in (c) and (d). (e) dI/dV spectra recorded over l -NO (purple) and over the clean surface (green). The tip position is shown in (b). The dI/dV for l -NO exhibits a distinct dip centered at 0 mV. The black curve is the fitting curve with the Fano function [Eq. (1)]. The tip height was fixed at $V_s = 50$ mV and $I = 0.1$ nA during each measurement. The spectra are vertically offset for clarity. Image size: 1.7×1.5 nm for (a)–(d).

that the dip is ascribed to the Kondo resonance, in which the tunneling path from the tip to the substrate is dominant. It is noted that l -NO is unstable above ~ 50 K, which hinders the measurement of the temperature dependence of the spectra. Because l -NO does not exist naturally on the surface, it is less stable than b -NO (metastable configuration) and can be attributed to the isolated on-top species described later.

V. DISCUSSION

A. Spectral shape variation between t -NO and l -NO

In Secs. IV B and IV E, we demonstrated that the STS for t -NO and l -NO exhibits the Kondo resonance with peak and dip shapes, respectively. The spectral shape is generally explained by the coupling strength between the orbital and tip [8,11]; if the coupling is strong (e.g., out-of-plane $2\pi_e^*$ orbital), the spectrum exhibits a peak, because the tunneling channel through the orbital is mainly dominant (large q). If the coupling is weak (e.g., in-plane $2\pi_o^*$ orbital), the spectrum exhibits a dip, owing to the contribution of the tunneling channel through the substrate (small q). The latter case is reported for NO/Au(111) [19]. In our case, the peak and dip structure observed in t -NO and l -NO would be attributed to the Kondo resonance hosted in the $2\pi_e^*$ and $2\pi_o^*$ orbitals, respectively.

We propose that the difference in the environment around the molecule determines the host of the Kondo resonance

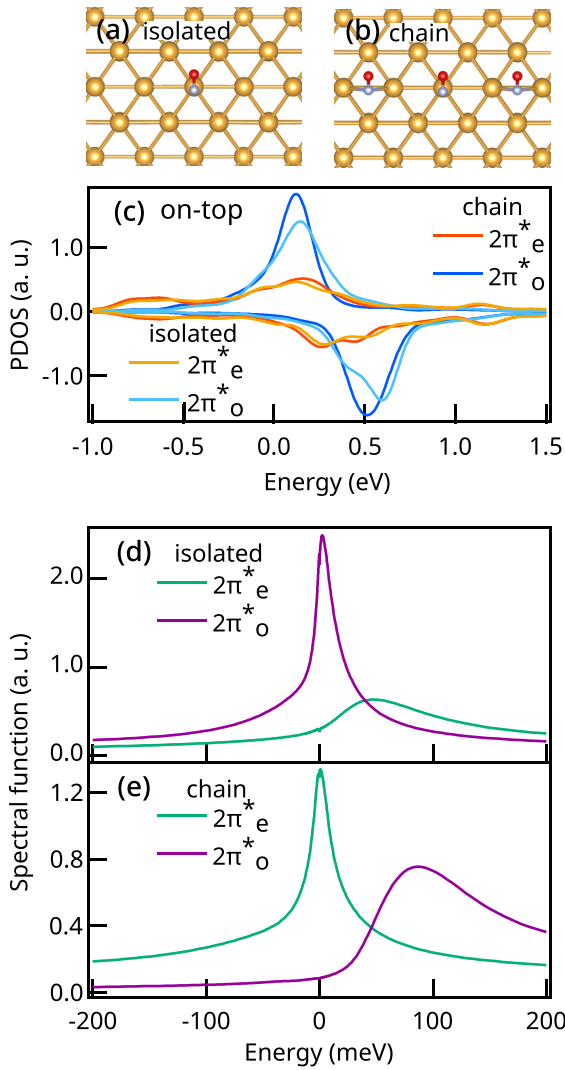


FIG. 6. (a, b) Top view of the calculated structure of the isolated on-top NO and the chain. (c) PDOS onto $2\pi_e^*$ and $2\pi_o^*$ for the on-top NO in the isolated form and that in the chain. The latter is the same as in Fig. 3(d). (d, e) Spectral functions calculated by NRG for isolated NO and that in the chain.

and, thus, the spectral shape. Figures 6(a) and 6(b) show the calculated structure of the isolated on-top NO and the chain, respectively. First, we assume the l -NO to be an isolated monomer on the on-top site. The reason is that the DFT reveals that the spin polarization is maintained for the on-top species, which is in agreement with the observation that l -NO exhibits Kondo resonance. We note that l -NO exhibits C_1 symmetry in the STM images (Fig. 5). The slight symmetry reduction observed in the STM image is not included in the theoretical model, as shown in Fig. 6(a). This is because it is difficult to determine the metastable low symmetric structure that perfectly matches l -NO in the structure optimization process in the DFT calculation. However, during the structure optimization calculations, we also find some intermediate structures where the N-O axis is slightly rotated in the $[1\bar{1}0]$ direction (Fig. S3) [41]. The total energies in these structures are higher than that of the symmetric on-top structure by approximately 20 meV. The magnetic moment of $0.36 \mu_B$ and

the shape of the DOS are similar to those of the symmetric on-top structure ($0.38 \mu_B$). This implies that the molecule can rotate around the on-top site with keeping the electronic and magnetic states.

Figure 6(c) shows the PDOS for the on-top NO in the isolated form and the chain. The PDOS for NO in the chain shows sharper peaks than that for the isolated one, and the peak position is shifted. These differences can be attributed to whether the bridge NO are adjacent or not, i.e., the surrounding environment. The PDOS indicates that both $2\pi_e^*$ and $2\pi_o^*$ are partially occupied. These suggest that this system is represented by the two-orbital Anderson model, in which either of the two orbitals can host the Kondo resonance [19].

Based on the DFT calculation described above, we study the present system by NRG calculation of the two-orbital Anderson model to determine whether $2\pi_e^*$ or $2\pi_o^*$ hosts the Kondo resonance, depending on the environment around the on-top NO. The Hamiltonian is as follows:

$$H = \epsilon_e n_e + \epsilon_o n_o + \sum_{\alpha=e,o} \sum_k (V_{k\alpha} c_{k\alpha}^\dagger c_\alpha + V_{k\alpha}^* c_\alpha^\dagger c_{k\alpha}) + H_{\text{int}}, \quad (2)$$

$$H_{\text{int}} = U_e n_{e\uparrow} n_{e\downarrow} + U_o n_{o\uparrow} n_{o\downarrow} + U_{eo} n_e n_o + J_H \mathbf{S}_e \cdot \mathbf{S}_o + W. \quad (3)$$

The first and second terms of H represent the electrons in $2\pi_e^*$ and $2\pi_o^*$ orbitals, respectively. $V_{k\alpha}$ ($\alpha = e, o$) is the hybridization matrix of the surface state with $2\pi_\alpha^*$ orbital. Here we take the wide-band limit and neglect the wave number dependence in hybridization, $V_{k\alpha} = V_{e,o}$. The hybridization strength in each channel is parametrized by $\Gamma_{e,o} = \pi V_{e,o}^2/2$. The interaction Hamiltonian H_{int} consists of the two intraorbital and one interorbital Hubbard interactions (U terms), the Coulomb ferromagnetic (Hund's rule) exchange interaction (J_H term), and the pair hopping term W . We fixed the parameters U_e , U_o , and U_{eo} to be 2.0 eV, and J_H and W to be -0.8 eV and -0.1 eV, respectively, which were referred from the gas phase value as well as from the previous study on NO/Au(111) [19].

Figure 6(c) reveals that the peak width and center of the PDOS in the isolated form and in the chain are different. Therefore, we take $\Gamma_{e,o}$, ϵ_e , and ϵ_o as variables for the NRG calculation. First, we consider the isolated NO, where the $2\pi_o^*$ is close to half-filling and serves as the host of the Kondo effect. To represent this situation, we set the parameters $\epsilon_e = -0.9$ eV, $\epsilon_o = -0.95$ eV, $\Gamma_e = 0.225$ eV, and $\Gamma_o = 0.09$ eV. The spectral function for $2\pi_o^*$ calculated using these parameters exhibits a peak at 0 meV, as expected [Fig. 6(d)]. Next, we modify the parameters with the hybridization reduced as $\Gamma_e = 0.175$ eV, and $\Gamma_o = 0.07$ eV, and the energy positions changed as $\epsilon_e = -0.95$ eV and $\epsilon_o = -0.9$ eV to make $2\pi_e^*$ close to half filling. These parameters are intended to reproduce the case of t -NO. Figure 6(e) shows the corresponding spectral function for the $2\pi^*$ orbitals. In this case, the spectral function for $2\pi_e^*$ exhibits a peak at 0 meV. These results indicate that the host of the Kondo resonance readily switches from $2\pi_o^*$ to $2\pi_e^*$ by modifying the parameters. As described in Secs. IV B and IV E, the Kondo resonance in the $2\pi_e^*$ orbital results in a Lorentz-like peak, and that in $2\pi_o^*$ results in a dip. The above theoretical results qualitatively support that the orbital

hosting the Kondo effect switches critically, depending on the environment around the molecule.

VI. CONCLUSION

We study the magnetic property of NO on Au(110)-(1×2) using STM, STS, DFT, and NRG. NO exists on the surface in three adsorption states, namely, *b*-NO, *t*-NO, and *l*-NO. STS and DFT calculation reveal the correlation between the geometry and magnetic property of NO; the on-top species (*t*-NO and *l*-NO) possesses larger magnetic moment than the bridge species (*b*-NO) due to weaker interaction with the surface. In addition, *t*-NO demonstrates the coupling of the Kondo resonance with molecular vibrations. Finally, we argue the difference in the shape of the Kondo resonance between *t*-NO and *l*-NO using DFT and NRG, and propose that

the system obeys the two-orbital Anderson model, and that the host of Kondo resonance readily switches between $2\pi_o^*$ and $2\pi_e^*$, by environmental perturbation around the molecule. Our results shed light on the importance of local geometry in the magnetism of NO on metal surfaces.

ACKNOWLEDGMENTS

The calculations were performed using the following computer facilities: Institute for Solid State Physics (Kashiwa, Japan), Center for Computational Materials Science (Tohoku University, Sendai, Japan), and Research Center for Computational Science (Okazaki, Japan). This work was supported by JSPS KAKENHI Grants No. 18K05030 and No. 19J15306, and by JST, CREST Grant No. JPMJCR20R4, Japan.

-
- [1] A. Yoshimori, Does a localized spin of adsorbed NO survive on Cu(111)? *Surf. Sci.* **342**, L1101 (1995).
- [2] I. Kinoshita, A. Misu, and T. Munakata, Electronic excited state of NO adsorbed on Cu(111): A two photon photoemission study, *J. Chem. Phys.* **102**, 2970 (1995).
- [3] M. P. Jigato, D. A. King, and A. Yoshimori, The chemisorption of spin polarised NO on Ag {111}, *Chem. Phys. Lett.* **300**, 639 (1999).
- [4] Q. Ge and D. King, Energetics, geometry and spin density of NO chemisorbed on Pt{111}, *Chem. Phys. Lett.* **285**, 15 (1998).
- [5] K. C. Hass, M.-H. Tsai, and R. V. Kasowski, Magnetic consequences of NO chemisorption on (100) metal surfaces, *Phys. Rev. B* **53**, 44 (1996).
- [6] J. Li, W.-D. Schneider, R. Berndt, and B. Delley, Kondo Scattering Observed at a Single Magnetic Impurity, *Phys. Rev. Lett.* **80**, 2893 (1998).
- [7] V. Madhavan, W. Chen, T. Jamneala, M. F. Crommie, and N. S. Wingreen, Tunneling into a single magnetic atom: Spectroscopic evidence of the Kondo resonance, *Science* **280**, 567 (1998).
- [8] M. Ternes, A. J. Heinrich, and W.-D. Schneider, Spectroscopic manifestations of the Kondo effect on single adatoms, *J. Phys. Condens. Matter* **21**, 053001 (2008).
- [9] A. Zhao, Q. Li, L. Chen, H. Xiang, W. Wang, S. Pan, B. Wang, X. Xiao, J. Yang, J. G. Hou, and Q. Zhu, Controlling the Kondo effect of an adsorbed magnetic ion through its chemical bonding, *Science* **309**, 1542 (2005).
- [10] E. Minamitani, N. Tsukahara, D. Matsunaka, Y. Kim, N. Takagi, and M. Kawai, Symmetry-Driven Novel Kondo Effect in a Molecule, *Phys. Rev. Lett.* **109**, 086602 (2012).
- [11] T. Komeda, Spins of adsorbed molecules investigated by the detection of Kondo resonance, *Surf. Sci.* **630**, 343 (2014).
- [12] A. Mugarza, R. Robles, C. Krull, R. Korytár, N. Lorente, and P. Gambardella, Electronic and magnetic properties of molecule-metal interfaces: Transition-metal phthalocyanines adsorbed on Ag(100), *Phys. Rev. B* **85**, 155437 (2012).
- [13] V. Iancu, A. Deshpande, and S.-W. Hla, Manipulation of the Kondo Effect Via Two-Dimensional Molecular Assembly, *Phys. Rev. Lett.* **97**, 266603 (2006).
- [14] J. Granet, M. Sicot, I. C. Gerber, G. Kremer, T. Pierron, B. Kierren, L. Moreau, Y. Fagot-Revurat, S. Lamare, F. Chérioux, and D. Malterre, Adsorption-induced Kondo effect in metal-free phthalocyanine on Ag(111), *J. Phys. Chem. C* **124**, 10441 (2020).
- [15] R. Tuerhong, M. Boero, and J.-P. Bucher, Molecular attachment to a microscope tip: Inelastic tunneling, Kondo screening, and thermopower, *Beilstein J. Nanotechnol.* **10**, 1243 (2019).
- [16] D. Jacob, M. Soriano, and J. J. Palacios, Kondo effect and spin quenching in high-spin molecules on metal substrates, *Phys. Rev. B* **88**, 134417 (2013).
- [17] Y. Jiang, Y. N. Zhang, J. X. Cao, R. Q. Wu, and W. Ho, Real-space imaging of Kondo screening in a two-dimensional O₂ lattice, *Science* **333**, 324 (2011).
- [18] S. Müllegger, M. Rashidi, M. Fattinger, and R. Koch, Surface-supported hydrocarbon π radicals show Kondo behavior, *J. Phys. Chem. C* **117**, 5718 (2013).
- [19] R. Requist, S. Modesti, P. P. Baruselli, A. Smogunov, M. Fabrizio, and E. Tosatti, Kondo conductance across the smallest spin 1/2 radical molecule, *Proc. Natl. Acad. Sci. USA* **111**, 69 (2014).
- [20] J. Liu, H. Isshiki, K. Katoh, T. Morita, B. K. Breedlove, M. Yamashita, and T. Komeda, First observation of a Kondo resonance for a stable neutral pure organic radical, 1, 3, 5-triphenyl-6-oxoverdazyl, adsorbed on the Au(111) surface, *J. Am. Chem. Soc.* **135**, 651 (2013).
- [21] I. Fernández-Torrente, K. J. Franke, and J. I. Pascual, Vibrational Kondo Effect in Pure Organic Charge-Transfer Assemblies, *Phys. Rev. Lett.* **101**, 217203 (2008).
- [22] S. Karan, N. Li, Y. Zhang, Y. He, I.-P. Hong, H. Song, J.-T. Lü, Y. Wang, L. Peng, K. Wu *et al.*, Spin Manipulation by Creation of Single-Molecule Radical Cations, *Phys. Rev. Lett.* **116**, 027201 (2016).
- [23] R. Temirov, A. Lassise, F. B. Anders, and F. S. Tautz, Kondo effect by controlled cleavage of a single-molecule contact, *Nanotechnology* **19**, 065401 (2008).
- [24] T. Choi, S. Bedwani, A. Rochefort, C.-Y. Chen, A. J. Epstein, and J. A. Gupta, A single molecule Kondo switch: Multistability of tetracyanoethylene on Cu(111), *Nano Lett.* **10**, 4175 (2010).
- [25] F. Eickhoff, E. Kolodzeiski, T. Esat, N. Fournier, C. Wagner, T. Deilmann, R. Temirov, M. Rohlfing, F. S. Tautz, and F. B. Anders, Inelastic electron tunneling spectroscopy for probing

- strongly correlated many-body systems by scanning tunneling microscopy, *Phys. Rev. B* **101**, 125405 (2020).
- [26] W. A. Brown and D. A. King, NO chemisorption and reactions on metal surfaces: A new perspective, *J. Phys. Chem. B* **104**, 2578 (2000).
- [27] A. Shiotari, T. Mitsui, H. Okuyama, S. Hatta, T. Aruga, T. Koitaya, and J. Yoshinobu, Configuration change of NO on Cu(110) as a function of temperature, *J. Chem. Phys.* **140**, 214706 (2014).
- [28] A. Shiotari, H. Koshida, and H. Okuyama, Adsorption and valence electronic states of nitric oxide on metal surfaces, *Surf. Sci. Rep.* **76**, 100500 (2021).
- [29] G. Binnig, H. Rohrer, C. Gerber, and E. Weibel, (111) facets as the origin of reconstructed Au(110) surfaces, *Surf. Sci.* **131**, L379 (1983).
- [30] G. Kresse and J. Furthmüller, Efficient iterative schemes for *ab initio* total-energy calculations using a plane-wave basis set, *Phys. Rev. B* **54**, 11169 (1996).
- [31] G. Kresse and J. Furthmüller, Efficiency of *ab-initio* total energy calculations for metals and semiconductors using a plane-wave basis set, *Comput. Mater. Sci.* **6**, 15 (1996).
- [32] P. E. Blöchl, Projector augmented-wave method, *Phys. Rev. B* **50**, 17953 (1994).
- [33] J. Klimeš, D. R. Bowler, and A. Michaelides, Van der Waals density functionals applied to solids, *Phys. Rev. B* **83**, 195131 (2011).
- [34] K. Momma and F. Izumi, VESTA 3 for three-dimensional visualization of crystal, volumetric and morphology data, *J. Appl. Crystallogr.* **44**, 1272 (2011).
- [35] E. Minamitani, Y.-S. Fu, Q.-K. Xue, Y. Kim, and S. Watanabe, Spatially extended underscreened Kondo state from collective molecular spin, *Phys. Rev. B* **92**, 075144 (2015).
- [36] R. Hiraoka, E. Minamitani, R. Arafune, N. Tsukahara, S. Watanabe, M. Kawai, and N. Takagi, Single-molecule quantum dot as a Kondo simulator, *Nat. Commun.* **8**, 16012 (2017).
- [37] F. B. Anders and A. Schiller, Spin precession and real-time dynamics in the Kondo model: Time-dependent numerical renormalization-group study, *Phys. Rev. B* **74**, 245113 (2006).
- [38] R. Peters, T. Pruschke, and F. B. Anders, Numerical renormalization group approach to Green's functions for quantum impurity models, *Phys. Rev. B* **74**, 245114 (2006).
- [39] C. Xu, C.-I. Chiang, Z. Han, and W. Ho, Nature of Asymmetry in the Vibrational Line Shape of Single-Molecule Inelastic Electron Tunneling Spectroscopy with the STM, *Phys. Rev. Lett.* **116**, 166101 (2016).
- [40] A. Shiotari, Y. Kitaguchi, H. Okuyama, S. Hatta, and T. Aruga, Imaging Covalent Bonding Between Two NO Molecules on Cu(110), *Phys. Rev. Lett.* **106**, 156104 (2011).
- [41] See Supplemental Material at <http://link.aps.org/supplemental/10.1103/PhysRevB.103.155412> for Kondo temperature for t-NO, and calculated structure and PDOS for isolated NO; which includes Ref. [53].
- [42] Z. Wu, L. Xu, W. Zhang, Y. Ma, Q. Yuan, Y. Jin, J. Yang, and W. Huang, Structure sensitivity of low-temperature NO decomposition on Au surfaces, *J. Catal.* **304**, 112 (2013).
- [43] M. Allan, Transitions Between the ${}^2\Pi_{1/2}$ and ${}^2\Pi_{3/2}$ Spin-Orbit Components of NO Induced by Impact of Slow Electrons, *Phys. Rev. Lett.* **93**, 063201 (2004).
- [44] M. Allan, Electron collisions with NO: Elastic scattering, vibrational excitation and ${}^2\Pi_{1/2} \rightleftharpoons {}^2\Pi_{3/2}$ transitions, *J. Phys. B* **38**, 603 (2005).
- [45] M. Ternes, Spin excitations and correlations in scanning tunneling spectroscopy, *New J. Phys.* **17**, 063016 (2015).
- [46] M. Ternes, Probing magnetic excitations and correlations in single and coupled spin systems with scanning tunneling spectroscopy, *Prog. Surf. Sci.* **92**, 83 (2017).
- [47] Z.-Z. Chen, H. Lu, R. Lü, and B.-F. Zhu, Phonon-assisted Kondo effect in a single-molecule transistor out of equilibrium, *J. Phys. Condens. Matter* **18**, 5435 (2006).
- [48] W. Ho, Single-molecule chemistry, *J. Chem. Phys.* **117**, 11033 (2002).
- [49] N. Lorente and M. Persson, Theory of Single Molecule Vibrational Spectroscopy and Microscopy, *Phys. Rev. Lett.* **85**, 2997 (2000).
- [50] N. Lorente, M. Persson, L. J. Lauhon, and W. Ho, Symmetry Selection Rules for Vibrationally Inelastic Tunneling, *Phys. Rev. Lett.* **86**, 2593 (2001).
- [51] S. R. Burema, N. Lorente, and M.-L. Bocquet, A theoretical rationalization of a total inelastic electron tunneling spectrum: The comparative cases of formate and benzoate on Cu(111), *J. Chem. Phys.* **136**, 244507 (2012).
- [52] A. Shiotari, H. Okuyama, S. Hatta, T. Aruga, M. Alducin, and T. Frederiksen, Role of valence states of adsorbates in inelastic electron tunneling spectroscopy: A study of nitric oxide on Cu(110) and Cu(001), *Phys. Rev. B* **94**, 075442 (2016).
- [53] K. Nagaoka, T. Jamneala, M. Grobis, and M. Crommie, Temperature Dependence of a Single Kondo Impurity, *Phys. Rev. Lett.* **88**, 077205 (2002).